PCCP

Elucidating the Interplay of Local and Mesoscale Ion Dynamics and Transport Properties in Aprotic Ionic Liquids

Journal:	*Physical Chemistry Chemical Physics*
Manuscript ID	CP-ART-12-2022-005863.R1
Article Type:	Paper
Date Submitted by the Author:	03-Feb-2023
Complete List of Authors:	Cosby, Tyler; The University of Tennessee Southern, Mathematics and Sciences Stachurski, Christopher; US Naval Academy Chemistry Department Mantz, Robert; US Army Research Office Trulove, Paul; US Naval Academy Chemistry Department Durkin, David ; US Naval Academy Chemistry Department

SCHOLARONE™
Manuscripts

PCCP

ARTICLE TYPE

Elucidating the Interplay of Local and Mesoscale Ion Dynamics and Transport Properties in Aprotic Ionic Liquids[†]

Tyler Cosby,[*a], Christopher D. Stachurski,[c‡] Robert A. Mantz,[b] Paul C. Trulove,[c] and David P. Durkin,[*c]

Ion dynamics and charge transport in 1-methyl-3-octylimidazolium ionic liquids with chloride, bromide, tetrafluoroborate, tricyanomethanide, hexafluorophosphate, triflate, tetrachloroaluminate, bis(trifluoromethylsulfonyl)imide, and heptachlorodialuminate anions are investigated by broadband dielectric spectroscopy, rheology, viscometry, and differential scanning calorimetry. A detailed analysis reveals an anion and temperature-dependent separation of characteristic molecular relaxation rates extracted from various representations of the dielectric spectra. The separation in rates extracted from the electric modulus and conductivity formalisms is interpreted as an experimental signature of significant heterogeneity in the local ion dynamics associated with the structural glass transition, viscosity, and dc ion conductivity. It is further found that the degree of dynamic heterogeneity correlates with the strengths of slow dielectric and mechanical relaxations previously attributed to the dynamics of mesoscale solvophobic aggregates. Increasing local dynamic heterogeneity correlates with an increase in the strength of the slow, aggregate dielectric relaxation and a decrease in the strength of the slow, aggregate mechanical relaxation. Accordingly, increasing local dynamic heterogeneity, brought about by change in temperature and/or cation/anion chemical structure, correlates with an increase in the static dielectric permittivities and a decrease in the contribution of aggregate dynamics to the zero-shear viscosities. The established correlation provides a new ability to distinguish between the influence of mesoscale aggregate shape/morphology *versus* local and mesoscale ion dynamics on the transport properties of ionic liquids.

1 Introduction

Ionic liquids (ILs) are wholly ionic materials consisting of molecular/atomic cations and anions with melting points below 100 °C.[1] Depending upon the particular combination of chemical structure of the cations and anions, ILs may exhibit a broad range of physicochemical properties, e.g., ionic conductivities, viscosities, static dielectric permittivities and solvating abilities which make them uniquely suited for widespread applications including electrochemical energy generation and storage, chemical synthesis, catalysis, gas absorption, and lubrication. The properties of an ionic liquid depend upon a complex interplay of local cation/anion intermolecular interactions and dynamics as well as,

in the case of ILs in which one or both ions possess extended apolar moities, longer-range mesoscale solvophobic organization and dynamics.[2–7] The ability to rationally design ILs for particular applications, i.e., tuning the physicochemical properties within a desired target range, relies upon developing a detailed understanding of the influence of chemical structure and temperature upon ion dynamics over broad length and time-scales and elucidating how these factors interplay and produce the resultant transport properties.[8,9] Among the properties of strongest interest are the ionic conductivities, viscosities, and static dielectric permittivities, properties which are crucial for the application of ILs as electrolytes, lubricants, and solvents. In this work, we perform a detailed investigation of local and mesoscale ion dynamics by broadband dielectric spectroscopy, rheology, viscometry, and differential scanning calorimetry. From a comprehensive analysis of the data, we (i) present new dielectric evidence of localized dynamic heterogeneity in aprotic ionic liquids, (ii) examine the influence of anion chemical structure and temperature on the observed degree of dynamic heterogeneity, and (iii) probe the apparent impact of dynamic heterogeneity on the mesoscale solvo-

[a] *Division of Mathematics and Sciences, University of Tennessee Southern, Pulaski, TN, USA. E-mail:jcosby3@utsouthern.edu*

[b] *Army Research Office, Durham, NC, USA.*

[c] *Department of Chemistry, US Naval Academy, Annapolis, MD, USA. E-mail: durkin@usna.edu*

phobic aggregate dynamics.

Ion dynamics in ionic liquids have been the subject of numerous investigations employing a wide variety of experimental and computational techniques including, but not limited to, broadband dielectric spectroscopy, rheology, depolarized dynamic light scattering, nuclear magnetic resonance spectroscopy, neutron spin echo spectroscopy, quasielastic neutron scattering, and molecular dynamics simulations.[10–22] These techniques are capable of probing contributions to ion dynamics over wide length and timescales and the experimental results have been attributed to such motions as ion librations, cage-rattling, ion diffusion, dipole reorientation, structural relaxation, and mesoscale solvophobic aggregate dynamics. One general finding which has emerged from these studies is a close coupling between the rates/timescales associated with ion diffusion, probed by dielectric spectroscopy and NMR, and the structural relaxation, determined from rheology. The coupling of these dynamics indicates ion conduction in ILs occurs via a glass-transition assisted mechanism where the limiting rate to ion diffusion is the dynamic glass transition.[23]

Of the previously mentioned techniques, neutron spectroscopies and molecular dynamics simulations provide simultaneous insight into both the timescale and lengthscale of dynamics. For instance, in neutron spin echo experiments the separation in timescales of the correlation decays in the pre-peak ($q_{\text{pre-peak}}$) and charge alternation peak (q_{ion}) reveal directly the motions of the mesoscale solvophobic aggregates and ion diffusion processes, respectively.[17,18] A comparable result was achieved in a recent MD simulation study by Amith and coworkers where it was shown that distinct dynamics of localized nearest neighbor and second nearest neighbor dynamics can also be resolved, corresponding to the timescales of the decay in the adjacency (q_{adj}) and charge alternation peaks (q_{ion}) of the scattering profile, respectively.[21,24]

These studies lead to several unanswered questions regarding ion dynamics in ionic liquids. For example it is unknown how the dynamics at the different lengthscales, i.e., those corresponding to the adjacency (nearest neighbor), ion (2nd nearest neighbor), and polarity alternation (mesoscale solvophobic aggregate) peaks, depend upon the cation/anion chemical structure. That is, certain cation/anion combinations may or may not have a greater or lesser degree of separation in the rates (timescales) of nearest neighbor, second nearest neighbor, and mesoscale solvophobic aggregate dynamics. Finally, it is unclear at present how the transport properties are influenced by these various dynamics. How do the dynamics spanning the various length/timescales collectively contribute to the viscosity, conductivity, and static dielectric permittivity? Finally, what is the role of cation/anion chemical structure on the collective contributions to the transport properties?

In order to provide insight into these questions, in this work the dynamics of a series of 1-methyl-3-octylimidazolium ILs with varying anion chemistries are investigated over broad temperature and frequency ranges by broadband dielectric spectroscopy, rheology, viscometry, and differential scanning calorimetry. A detailed analysis of the dielectric spectra reveals a significant separation in rates associated with both local ion dynamics and mesoscale solvophobic aggregate dynamcis. By comparison with

those rates obtained by Amith the rates associated with local dynamics are tentatively attributed to translational ion motions at lengthscales of nearest neighbor and second nearest neighbor correlations. It is further found that the degree of separation in the local ion dynamics is highly dependent on the anion chemistry as well as the temperature. While certain ILs have distinctly heterogeneous local ion dynamics at elevated temperatures (i.e., well-separated rates/timescales of local ion motions), at low temperatures and for certain ion chemistries the local ion dynamics become less heterogeneous as evidenced by a merging of the dynamics at the two rates/lengthscales. Finally, the degree of local dynamic heterogeneity, measured by the separation in rates, is shown to have important implications for the slow dielectric and mechanical relaxations associated with mesoscale solvophobic aggregate dynamics. There is an especially strong correlation between the separation in rates and the strength of the slow dielectric relaxation, resulting in drastically diminished static dielectric permittivities for those ILs with the smallest degree of separation in rates of local ion dynamics.

2 Materials and Methods

2.1 Source and Purity of Materials

1-methyl-3-octylimidazolium bromide (C_8MIm Br, >99%), 1-methyl-3-octylimidazolium tetrafluoroborate (C_8MIm BF_4, >99%), 1-methyl-3-octylimidazolium hexafluorophosphate (C_8MIm PF_6, >99%), 1-methyl-3-octylimidazolium tricyanomethanide (C_8MIm TCM, >98%), 1-methyl-3-octylimidazolium bis(trifluoromethylsulfonyl)imide (C_8MIm TFSI, >99%), 1-methyl-3-octylimidazolium trifluoromethanesulfonate (C_8MIm triflate, >99%) were purchased from Iolitec and used as received.

1-chlorooctane (99%), 1-methylimidazole (99%), acetonitrile ($\geq$ 99%), sodium chloride ($\geq$ 99.9%), and butyl acetate ($\geq$ 99%) were purchased from Sigma Aldrich. The 1-methylimidazole was further purified by vacuum distillation prior to use. Ethyl acetate ($\geq$ 99.8%) was purchased from Pharmco. Aluminum chloride (>97% purity) was purchased from Honeywell Fluka and further purified by sublimation in a sealed glass bomb tube containing aluminum wire and sodium chloride.[25,26] Following sublimation the expected purity is >99.9%.[25,26] Aluminum wire (>99.99%) was purchased from Alfa Aesar.

2.2 IL Synthesis

The chloroaluminate ionic liquids were prepared by slowly adding 1-methyl-3-octylimidazolium chloride (C_8MIm Cl) to aluminum chloride ($AlCl_3$) with stirring at room temperature until a clear homogeneous liquid was formed. The mixture compositions were fixed at a 1:1 and 2:1 mole ratio of $AlCl_3$ to C_8MIm Cl for all chloroaluminate ionic liquids examined in this study. At this ratio, the reaction between $AlCl_3$ and the chloride anions yields an IL consisting predominantly of tetrachloroaluminate ($AlCl_4^-$) and heptachlorodialuminate ($Al_2Cl_7^-$) anions, respectively. Therefore, the IL names are abbreviated to C_8MIm $AlCl_4$ and C_8MIm Al_2Cl_7 throughout. The 1-methyl-3-octylimidazolium chloride starting material was synthesized by gently refluxing 1-methylimidazole

and the 1-chlorooctane in acetonitrile. Due to its low (or absent) melting points, the 1-methyl-3-octylimidazolium chloride salt was rinsed thoroughly with butyl acetate, rather than recrystallized, and then dried on a high vacuum line. The purity of the starting C_8MIm Cl salt, determined by ^{1}H and ^{13}C NMR, was $\geq$99.9% purity, the NMR spectra are provided in the Supplementary Information. The corresponding purities of the C_8MIm $AlCl_4$ and C_8MIm Al_2Cl_7 ILs is ($\geq$99%).

The chloroaluminate ionic liquids are highly moisture sensitive. To exclude the effect of water contamination all mixtures were prepared in a nitrogen atmosphere glove box ($H_2O<1$ ppm). DSC samples were loaded into hermetically sealed aluminum pans in the same glove box and measured immediately afterward. The dielectric measurements of all ILs were performed within a cryostat which was constantly purged with dry nitrogen gas from a liquid nitrogen dewar. Dielectric sample capacitors were held in a plastic bag and purged with dry nitrogen gas for one hour prior to filling with a sealed syringe containing the ionic liquid sample. The sample capacitor was then lowered into the cryostat while continuously purging with dry nitrogen. For the rheological measurements, the rheometer was housed in a home-built glovebox which was thoroughly and continuously purged with dry nitrogen supplied by a liquid nitrogen cylinder. In both the dielectric and rheology experiments reproducible results were obtained which exclude any effect of water uptake.

2.3 Broadband Dielectric Spectroscopy

Broadband dielectric spectroscopy measurements were made over the frequency range $f = 10^{-1} - 10^9$ Hz. Measurements from $10^{-1} - 3 \times 10^6$ Hz were made using a Novocontrol α-analyzer with a parallel plate capacitor geometry consisting of 20 mm diameter gold-plated brass electrodes and a 1.0 mm sample thickness maintained by Teflon spacers. Measurements from $10^6 - 10^9$ Hz were made on a HP E4991B impedance analyzer with Novocontrol RF extension and a parallel plate sample capacitor geometry consisting of 10 mm diameter gold-plated brass electrodes and a 0.1 mm sample thickness maintained by 100 μm fused silica rod spacers. Temperature control for all BDS measurements was provided by a Quatro temperature control system using nitrogen as a cooling and heating gas. The temperature accuracy was $\pm$0.1 °C.

2.4 Shear Rheology

Steady-shear and small-amplitude oscillatory shear rheology measurements were performed on a TA Instruments HR-2 rheometer with temperature control provided by an Environmental Test Chamber accurate within $\pm$0.1 °C. Samples were filled between parallel stainless steel plates of 25 mm and 8 mm diameter. The oscillatory shear measurements were performed with the 8 mm plates over the frequency range 1-100 Hz with 0.05 - 2% strain.

2.5 Differential Scanning Calorimetry

Differential scanning calorimetry (DSC) measurements were performed on a TA instruments Q2000 calorimeter. Samples were encased in TZero aluminum hermetic pans and subjected to heat-

ing and cooling scans at a rate of 10°C/min. Calorimetric glass transition temperatures (T_g) were recorded on cooling and correspond to a maximum in the temperature derivative of heat flow.

3 Results and Discussion

The chemical structures of the investigated ILs are provided in Figure 1. All the ILs share the common 1-methyl-3-octylimidazolium (C_8MIm) cation with varying anion chemical structure as shown. The anion abbreviations used throughout are provided in the Figure 1 caption as well as the Experimental Methods.

3.1 Differential Scanning Calorimetry

The calorimetric glass transition temperatures recorded on cooling are as follows: C_8MIm Cl ($T_g = 227$ K), C_8MIm Br (211 K), C_8MIm BF_4 (192 K), C_8MIm PF_6 (200 K), C_8MIm triflate (N/A), C_8MIm $AlCl_4$ (183 K), C_8MIm TFSI (186 K), C_8MIm Al_2Cl_7 (179 K). The C_8MIm triflate IL crystallized at 223 K. The calorimetric heating/cooling curves are provided in the Supplementary Information.
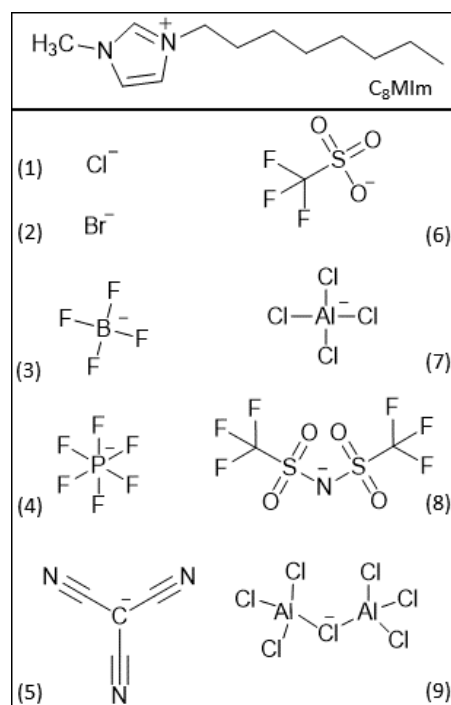

Fig. 1 Chemical structures of the investigated ionic liquids consisting of the 1-methyl-3-octylimidazolium cation and the (1) chloride, Cl, (2) bromide, Br, (3) tetrafluoroborate, BF_4, (4) hexafluorophosphate, PF_6, (5) tricyanomethanide, TCM, (6) triflate, (7) tetrachloroaluminate, $AlCl_4$, (8) bis(trifluoromethylsulfonyl)imide, TFSI, and (9) heptachlorodialuminate, Al_2Cl_7, anion.

3.2 Broadband Dielectric Spectroscopy

The frequency and temperature-dependent dielectric spectra of a representative IL C_8MIm PF_6 are presented in Figure 2 in terms of the real part of complex conductivity, $\sigma^*(\omega) = \sigma'(\omega) + i\sigma''(\omega)$, the imaginary part of the complex electric modulus, $M^*(\omega) =$

$M'(\omega)+iM''(\omega)$, and the derivative representation of the real part of complex dielectric permittivity, $\varepsilon^*(\omega) = \varepsilon'(\omega) - i\varepsilon''(\omega)$ where $\varepsilon''_{der}(\omega) = -\frac{\pi}{2}\frac{\partial\varepsilon'(\omega)}{\partial ln\omega}$. Each of these interrelated representations of the dielectric data emphasizes particular contributions of ion dynamics to the overall material response. By analyzing each representation in turn certain subtle aspects of ion dynamics may be elucidated.[27] The imaginary electric modulus, M'', and real conductivity, σ', representations especially emphasize contributions of translational ion motions while the derivative representation of the real part of complex dielectric permittivity, ε''_{der}, also contains significant contributions from both dipole reorientation as well as a type of supramolecular interfacial polarization due to the existence of mesoscale solvophobic aggregates.[11,28–30] To extract useful information regarding these ion dynamics, the dielectric spectra in each of the three representations are analyzed by applying appropriate fit functions outlined below. The dielectric spectra of all investigated ILs are provided in the Supplementary Information.

The plateau value of $\sigma'(\omega)$ is the DC ionic conductivity of the liquid, σ_0. At frequencies above the plateau, the value of σ' increases sharply, corresponding to a transition from DC to AC ion conductivity. The onset frequency of σ_0 corresponds to a transition from localized ion-hopping (AC conduction) to long-range ion diffusion (DC conduction). This transition is well described by the random barrier model (RBM), Eq. 1. In this model, charge transport is assumed to occur via ion-hopping within a randomly varying energy landscape.[31] The model contains only one free parameter, $\tau_{RBM} = \frac{1}{\omega_{RBM}}$, which is the time required for the ion to overcome the largest energy barrier and begin to undergo long-range diffusion. The original RBM, and updated versions, has been widely employed to investigate charge transport in ionic liquids as well as ion-conducting solids and polymers.[32–38]

$$\sigma^*(\omega) = \sigma_0\left[\frac{i\omega\tau_{RBM}}{\ln(1+i\omega\tau_{RBM})}\right] \quad (1)$$

The temperature-dependent maxima in $M''(\omega)$, usually termed the conductivity relaxation rate, is another commonly employed measure of ion dynamics in a wide variety of ion-conducting materials.[39,40] To extract the frequency of the maxima, the imaginary part of complex electric modulus, $M''(\omega)$, was fit by a single Havriliak-Negami equation:

$$\varepsilon^*(\omega) = \frac{\Delta\varepsilon_{M''}}{(1+(i\omega\tau_{HN,M''})^\beta)^\gamma} \quad (2)$$

The derivative representation of the real part of dielectric permittivity, $\varepsilon''_{der}(\omega)$, is utilized in order to suppress the contribution of σ_0 to the imaginary dielectric permittivity $\varepsilon''(\omega)$. This representation has previously been utilized to reveal "hidden" contributions arising from the motion of mesoscale solvophobic aggregates in ILs containing amphiphilic ions.[11,30,41] This mesoscale dielectric relaxation is observed as an additional low-frequency peak or shoulder at frequencies below that of the primary α dielectric relaxation which is associated with local ion dynamics including contributions from both translational and dipole reorientational ion motions. The $\varepsilon''_{der}(\omega)$ spectra are well-described by
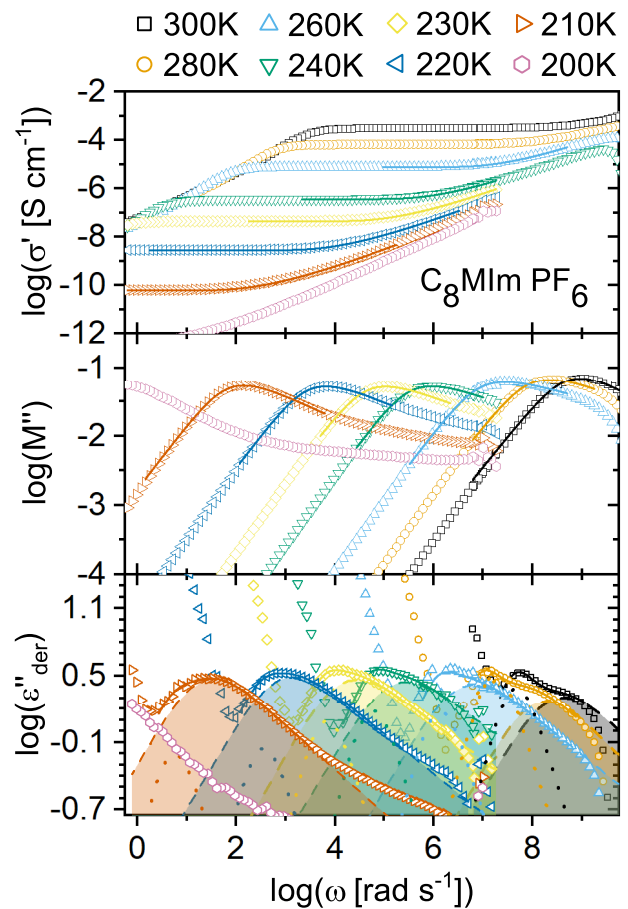

Fig. 2 Frequency, $\omega = 2\pi f$, and temperature-dependent dielectric spectra of $C_8MIm\ PF_6$. (Top) Real part of complex conductivity, $\sigma'(\omega)$. Lines represent fits by the RBM. (Middle) Imaginary part of complex electric modulus, $M''(\omega)$. Lines represent fits by a single Havriliak-Negami (HN) function. (Bottom) Derivative representation of the real part of complex dielectric permittivity, ε''_{der}. Solid lines represent the total fit obtained by a combination of two HN functions. The separate component HN fit functions are presented as dashed and dotted lines. The shaded areas depict the contribution of the primary, α dielectric relaxation.

a combination of two Havriliak-Negami equations:

$$\varepsilon^*(\omega) = \varepsilon_\infty + \frac{\Delta\varepsilon_\alpha}{(1+(i\omega\tau_{HN,\alpha})^\beta)^\gamma} + \frac{\Delta\varepsilon_{sub-\alpha}}{(1+(i\omega\tau_{HN,sub-\alpha})^\beta)^\gamma} \quad (3)$$

where ε_∞ is the high-frequency limiting value of permittivity, $\Delta\varepsilon$ is the dielectric strength, τ is the model relaxation time, and β and γ are shape parameters. Note that in all cases the dielectric permittivity spectra were fit in the real part, $\varepsilon'(\omega)$. The fit lines were then re-cast into the derivative representation in order to better illustrate the different relaxations contributing to the dielectric permittivity spectra.

The molecular relaxation rates, $\omega_{M''}$, ω_α, and $\omega_{sub-\alpha}$, are calculated by Equation 4 using the corresponding Havriliak-Negami fit parameters of Equations 2 and 3.

$$\omega_{max} = \frac{1}{\tau_{HN}}[\sin(\frac{\beta\pi}{2+2\gamma})]^{1/\beta}[\sin\frac{\beta\gamma\pi}{2+2\gamma}]^{-1/\beta} \quad (4)$$

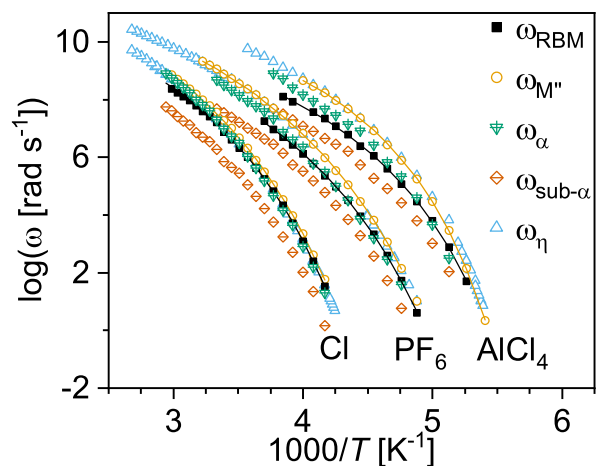The temperature-dependent relaxation rates thus extracted

Fig. 3 Temperature-dependent relaxation rates of the 1-octyl-3-methylimidazolium ILs with the indicated anions. Rates are obtained by analysis of the dielectric spectra (ω_{RBM}, $\omega_{M''}$, ω_α, $\omega_{sub-\alpha}$) and rheology (ω_η). Lines correspond to fits by the VFT equation.

from the dielectric and mechanical spectra of C_8MIm PF_6, C_8MIm Cl, and C_8MIm $AlCl_4$, are presented in Figure 3. All relaxation rates follow a temperature dependence well described by the Vogel-Fulcher-Tammann (VFT) equation. A primary effect of changing the anion chemical structure is a speeding up and shift of relaxation rates to lower temperatures. This speeding up of dynamics is also reflected in a shift in the calorimetric glass transition temperatures. This observation matches the generally observed trend that larger, more charge-diffuse anions tend to decrease the glass transition temperature in a series of ILs sharing a common cation.[10,42]

A more subtle effect of varying anion chemical structure on ion dynamics is observed by considering the separation in those rates characteristic of charge transport, namely, ω_{RBM} and $\omega_{M''}$. For instance, in C_8MIm Cl these two rates are found to very nearly overlay in Figure 3 while for C_8MIm PF_6 there is significant separation between the fastest rates, corresponding to $\omega_{M''}$, and the slowest rates, ω_{RBM}. The observed separation is even more exaggerated for C_8MIm $AlCl_4$. The degree of separation also has a pronounced temperature dependence; increasing separation with increasing temperature. The separation in the fastest and slowest measures of translational ion dynamics may also be plainly observed directly in the dielectric spectra. Figure 4 presents the dielectric spectra of C_8MIm Cl and C_8MIm Al_2Cl_7 plotted *versus* frequency normalized $\omega_{M''}$. As clearly evident in this representation, the peak in M'' is located at higher frequencies relative to the the onset frequency of the dc ionic conductivity plateau when the chloride anion is switched to heptachlorodialuminate. This is a clear indication that in certain imidazolium ILs the fastest translational ion motions become significantly separated from the final onset of long-range ion diffusion. We propose therefore that the degree of separation in the rates ω_{RBM} and $\omega_{M''}$ represents an important and presently underappreciated indication of the dynamical landscape in ionic liquids *where increasing separation indicates an increasingly heterogeneous local ion dynamics*. The

increased dynamic heterogeneity is also reflected in the width of the M'' peak, where the broader peak of C_8MIm Al_2Cl_7 indicates a broader distribution of underlying ion-hopping rates.[43] The anion-dependent width of the M'' peak is reflected in the shape parameters of the Havriliak-Negami function used to fit this peak, provided in the Supplementary Information.

To quantify the dependence of the separation in relaxation rates on temperature and anion chemical structure, in Figure 5 the ratio $\frac{\omega_{M''}}{\omega_{RBM}}$ is presented for all investigated ILs. The ratio is strongly dependent upon the temperature and anion structure. It is important to note that the degree of separation is characteristic of the anion/cation combination, but does not appear to depend strongly on the length of the alkyl chain on the imidazolium cation. A very similar degree of separation was reported for the short-chain, non-aggregating C_2MIm Al_2Cl_7 and C_4MIm Al_2Cl_7.[27] Accordingly, the separation is attributed to local ion dynamics mediated by intermolecular cation/anion interactions.

To better understand the separation in these relaxation rates in terms of ion motions we turn to a recent series of articles from Amith in which computational techniques were employed to interrogate the contributions of ion dynamics at local, intermediate, and mesoscopic lengthscales to the mechanical (viscous) relaxation of imidazolium ionic liquids with the bis(trifluoromethylsulfonyl)imide anion.[21,24] In these works, the authors emphasize that, at a given temperature, the three peaks observed in the x-ray and neutron scattering profiles of ionic liquids, peaks associated with local ion adjacency, ion-alternation, and polarity alternation correlations, respectively, decay at markedly differing timescales. To illustrate the close correspondence of these dynamics and the associated correlations we show in Figure 6 the relaxation rates obtained by dielectric spectroscopy, rheology, and viscometry, together with the rates of decorrelation for the adjacency, charge, and polarity correlations ($\omega_{q-adjacency}$, $\omega_{q-charge}$, and $\omega_{q-polarity}$, respectively) reproduced from Amith et. al.[21] The observed separation in $\omega_{q-adjacency}$, $\omega_{q-charge}$, and $\omega_{q-polarity}$ matches closely the separation in $\omega_{M''}$, ω_{RBM}, and $\omega_{sub-\alpha}$. In addition, we include decorrelation rates from neutron spin echo spectroscopy obtained for the low-q pre-peak and middle-q ion alternation peak.[17] We propose that in our experimental work using dielectric spectroscopy we are resolving the dynamics associated with these three distinct regimes. The fastest ion motions, corresponding to the decay in the local charge-adjacency correlation, contribute predominantly to the peak in the M''. The onset of dc ionic conductivity occurs when ions overcome their largest energy barrier and finally escape their local cages and thus the rate of the RBM corresponds to the decay in the charge-alternation correlation. Finally, the slowest decay reported by the prior authors, that associated with the decay in the polarity alternation correlation, corresponds with the polarization due to local fluctuations in charge density across mesoscopic aggregates, a dynamic process observed in the dielectric spectra as the sub-α relaxation in ε''_{der}.

As mentioned previously, the derivative spectra, ε''_{der}, of the C_8MIm ILs are dominated by two relaxations. The faster, primary, α-relaxation is attributed to a combination of dipole reorientation as well as ionic polarization due to translation ion motions.[44]
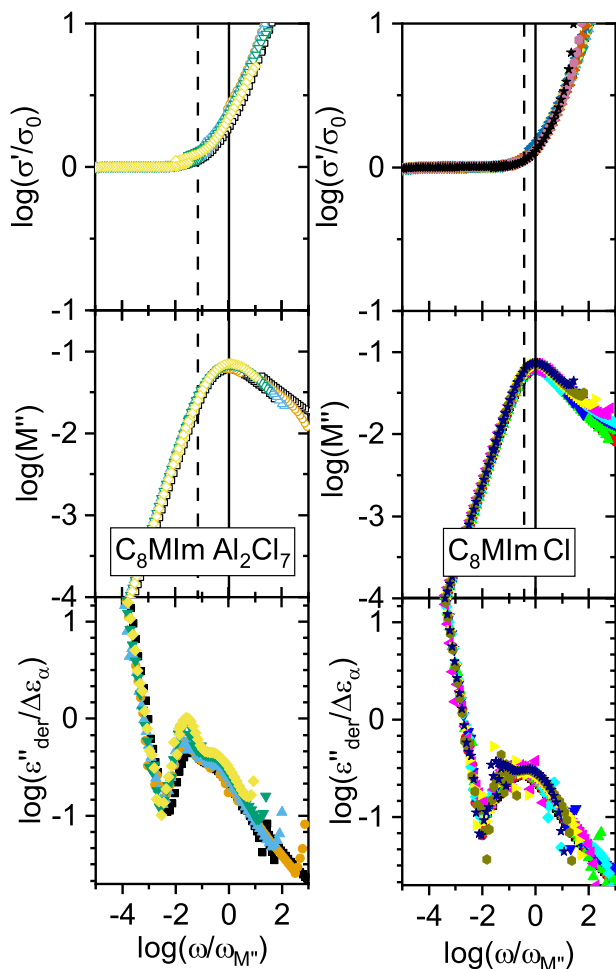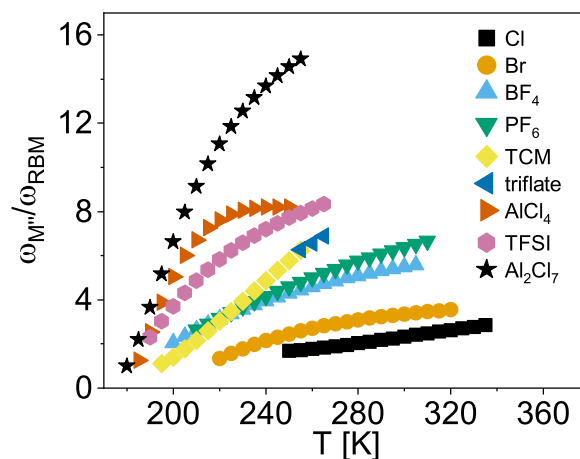
Fig. 5 Temperature dependent ratio of relaxation rates extracted from the imaginary part of the complex electric modulus, $\omega_{M''}$, and RBM-fits of the real part of complex conductivity, ω_{RBM}. Increasing separation of these respective relaxation rates is attributed to an increase in heterogeneity of local ion dynamics associated with decay in adjacency and charge alternation correlations. The relaxation rate ratio is calculated from the VFT fit equations

The slower, sub-α relaxation has been observed in a variety of ILs which exhibit organization at mesoscopic lengthscales due to solvophobic aggregation of polar and non-polar components of amphiphilic ions. The sub-α relaxation has previously been attributed to an interfacial polarization across such aggregates due to local fluctuations in charge density in polar regions separated by a non-polar region. The rates of these relaxations are presented in Figure 3. The primary, α-relaxation rate, ω_α, tends to coincide with ω_{RBM} at low temperatures and falls in between ω_{RBM} and $\omega_{M''}$ at elevated temperatures. The sub-α relaxation rate, $\omega_{sub-\alpha}$, is always well below ω_{RBM}.

In addition to the relaxation rates, the Havriliak-Negami fits of ε' also provide the strengths of the α and sub-α relaxations, $\Delta\varepsilon_\alpha$ and $\Delta\varepsilon_{sub-\alpha}$, respectively. These temperature-dependent dielectric strengths are provided in Figure 7 along with the high-frequency limiting permittivity, ε_∞. The inverse temperature dependence of $\Delta\varepsilon_\alpha$ follows the temperature dependent mass density and is typical of a molecular dipolar reorientation for non-correlated dipoles. The magnitude of $\Delta\varepsilon_\alpha$ exceeds predictions of the Onsager relation possibly due to an additional contribution from ionic polarization. The value of $\Delta\varepsilon_{sub-\alpha}$ for all ILs decreases with decreasing temperature. The unusual temperature dependence and very slow rates of this relaxation both indicate its supramolecular origin. The temperature dependence of $\Delta\varepsilon_{sub-\alpha}$ reported here for C_8MIm ILs is common to all ILs for which this relaxation has been observed. The origin of the temperature dependence is as yet unexplained. In prior investigations, shifts in $\Delta\varepsilon_{sub-\alpha}$ accompanying changes to ion chemical structure or composition were linked to changes in morphology of the mesoscale solvophobic aggregates.[11,30,45] The primary experimental evidence for mesoscale aggregation is the existence of a pre-peak in the x-ray and neutron scattering profiles of ILs with amphiphilic ions. The real-space distance associated with the pre-peak corresponds to the distance be-
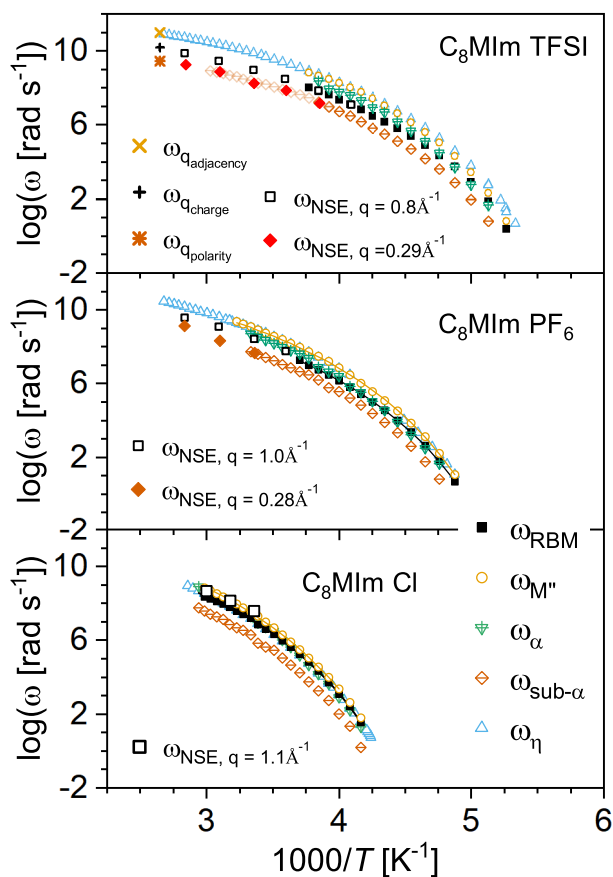

Fig. 4 Temperature-dependent dielectric spectra of C_8MIm Al_2Cl_7 (240-200 K) and C_8MIm Cl (320-240 K) *versus* frequency normalized by the peak-frequency of M″, $\omega_{M''}$. The solid lines correspond to $\omega = \omega_{M''}$. The dashed lines indicate the frequencies obtained by the RBM fit of σ' at the highest temperature data point for each IL.

Fig. 6 Temperature-dependent relaxation rates of C_8MIm TFSI, C_8MIm PF_6, and C_8MIm Cl. Rates are obtained by analysis of the dielectric spectra (ω_{RBM}, $\omega_{M''}$, ω_α, $\omega_{sub-\alpha}$) and rheology (ω_η). Faded crossed-diamond symbols are screen-read values of $\omega_{sub-\alpha}$. Decorrelation rates of the adjacency, charge alternation, and polarity correlations ($\omega_{q-adjacency}$, $\omega_{q-charge}$, $\omega_{q-polarity}$) are reproduced from the single-exponential fits of correlation decays obtained by molecular dynamics simulations by Amith.[24] Decorrelation rates from neutron spin echo spectroscopy at the indicated q-values are reproduced from Kofu.[17]

twen polar ionic phases separated by non-polar phases consisting of interdigitated alkyl chains. As the length of the alkyl chain increases, this distance becomes larger and $\Delta\varepsilon_{sub-\alpha}$ increases. Similarly, in mixtures of aggregating and non-aggregating ILs shifts in the pre-peak have been interpreted, on the basis of molecular dynamics simulations, as indicating a shift to increasingly spherical aggregates with dilution of the aggregating IL.[45] The transition in morphology was found to correlate with a substantial increase in $\Delta\varepsilon_{sub-\alpha}$, a finding consistent with the interfacial mechanism of the sub-α relaxation. It is, therefore, tempting to attribute the anion chemical structure and temperature dependence of $\Delta\varepsilon_{sub-\alpha}$ of the C_8MIm ILs to a similar shift in aggregate morphology or size. However, the q-values of the pre-peak reported in the literature for the C_8MIm Cl, C_8MIm BF_4, C_8MIm PF_6, C_8MIm TCM and C_8MIm TFSI, are very similar, ranging from 0.27 to 0.33 or a difference in real space distance of approximately 3.9 Å.[13,46–48] Furthermore, prior computational investigations of these ILs indicate the presence of morphologically similar aggregates described as consisting of bicontinuous polar and non-polar domains. Therefore, the temperature and anion-dependent changes in $\Delta\varepsilon_{sub-\alpha}$ do not appear to be linked primarily to aggregate size or morphology.

Interestingly, upon comparing the separation in local ion dynamics quantified by the ratio, $\frac{\omega_{M''}}{\omega_{RBM}}$ in Figure 3 with the $\Delta\varepsilon_{sub-\alpha}$ in Figure 7 we find they share precisely the same trend with both temperature and anion chemical structure. This fact is made more obvious by plotting $\Delta\varepsilon_{sub-\alpha}$ *versus* $\frac{\omega_{M''}}{\omega_{RBM}}$ in Figure 8. The data for all of the investigated pure ILs collapse onto a line. To show the universality of this relationship, we have added additional data from prior investigations of quaternary phosphonium ILs, $P_{2,2,2,8}$ TFSI and $P_{2,2,2,12}$ TFSI, additional chloroaluminate ILs, C_6MIm $AlCl_4$ and 60mol% $AlCl_3$ + C_6MIm Cl, as well as binary mixtures of C_2MIm BF_4 and C_8MIm BF_4.[11,27,30,45] The direct correlation between $\frac{\omega_{M''}}{\omega_{RBM}}$ and $\Delta\varepsilon_{sub-\alpha}$ holds for all ILs with the exception of the binary IL mixtures. In that case, by mixing the aggregating C_8MIm and non-aggregating C_2MIm cations the morphology of the solvophobic aggregates was altered from bicontinuous to isolated spherical aggregates as verified by x-ray scattering and molecular dynamics simulations.

The plot of $\Delta\varepsilon_{sub-\alpha}$ *versus* $\frac{\omega_{M''}}{\omega_{RBM}}$ therefore indicates a close coupling of the heterogeneity of local ion dynamics and the strength of the interfacial polarization responsible for the sub-α dielectric relaxation. The factors which influence the strength of interfacial polarizations are (i) the shape of the interfaces and the distance which separates them, (ii) the density of interfaces, and (iii) the mobility of the ions responsible for the local charge density fluctuations underlying the polarization.[11,27,30,45] Therefore, Figure 8 therefore represents a useful and previously unreported analytical tool for disentangling the influence of ion mobility from aggregate size and morphology effects on $\Delta\varepsilon_{sub-\alpha}$.

It is important to note that the heterogeneous ion dynamics which are evidenced by separation in $\omega_{M''}$ and ω_{RBM} is apparently distinct from the dynamic heterogeneity typically observed in glass forming liquids as the temperature approaches the calorimetric glass transition. One significant difference between the two types of dynamic heterogeneity is their opposite temperature dependence. In the present case, the observed local heterogeneity
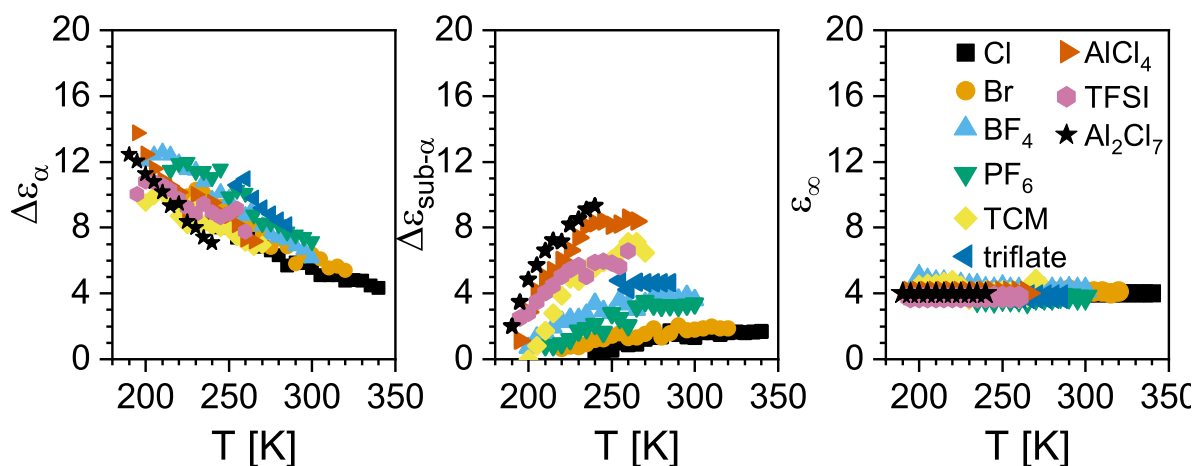
Fig. 7 Dielectric strengths of the α-relaxation, $\Delta\varepsilon_\alpha$, the slower sub-α relaxation, $\Delta\varepsilon_{\text{sub-}\alpha}$, and the high-frequency limiting dielectric permittivity, ε_∞ obtained by fitting the real part of dielectric permittivity with Equation 3.
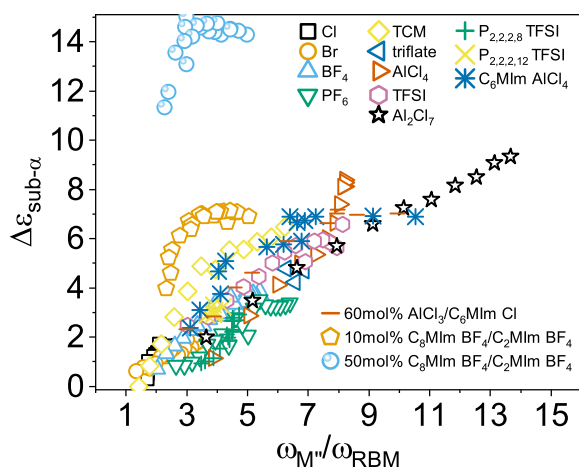

Fig. 8 Dielectric strength of the slower sub-α relaxation, $\Delta\varepsilon_{\text{sub-}\alpha}$, *versus* the ratio of relaxation rates $\omega_{M''}$ and ω_{RBM}. The $\Delta\varepsilon_{\text{sub-}\alpha}$ of a wide variety of pure ILs correlates closely with the ratio $\frac{\omega_{M''}}{\omega_{\text{RBM}}}$. Notable exceptions are the binary IL mixtures composed of C_2MIm BF_4 and C_8MIm BF_4, which are known to exhibit mesoscale solvophobic aggregates with a composition-dependent shape.

decreases as temperature is reduced. However, for the dynamic heterogeneity more typical of glass formers the heterogeneity increases as T_g is approached.[49,50] The distinction is possibly due to the relative spatial and temporal ranges of each type of dynamic heterogeneity. In the present case, the relevant lengthscale is at the nearest neighbor and next nearest neighbor while the heterogeneity near T_g may be at significantly longer lengthscales. Notably, recent dielectric investigations of other ILs have also revealed possible signatures of increased dynamic heterogeneity emerging near T_g in the $\varepsilon''_{\text{der}}$ representation.[27,32] However, for the mesoscopically aggregating C_8MIm ILs the sub-α relaxation obscures this signature.

3.3 Rheology

The small amplitude oscillatory shear rheology data are presented in Figure 9 in terms of the real and imaginary parts of complex

viscosity, $\eta^*(\omega) = \eta'(\omega) + \eta''(\omega)$. The master curves were constructed via time-temperature superposition. The primary mechanical relaxation appears as a peak in η''. The frequency of this peak corresponds to the structural relaxation rate of the liquid ω_η. The rates obtained by oscillatory rheology correspond to the lowest temperature ω_η data points in Figure 3. Previously, in C_8MIm Cl and C_8MIm BF_4 an additional slower mechanical relaxation was observed as a shoulder in η'' at frequencies below the structural relaxation.[11,45] Due to the slow rate of this process and its emergence only for long-chain imidazolium cations the process was attributed to dynamics of mesoscale solvophobic aggregates. The slow mechanical relaxation is also observed for the C_8MIm Br and C_8MIm PF_6 ILs while it is absent from the mechanical response of C_8MIm TCM, C_8MIm $AlCl_4$, C_8MIm TFSI, and C_8MIm Al_2Cl_7. The strength of the slow mechanical relaxation decreases in the order Br $\approx$ BF_4 > Cl > PF_6. In contrast to the sub-α dielectric relaxation, the slow mechanical relaxation shows no obvious temperature dependence within the limited temperature range available from the instrumental technique employed. This contrast between the dielectric and mechanical response highlights different mechanisms which underlie the dielectric and mechanical supramolecular relaxations. Considering the series of anions which exhibit the supramolecular mechanical relaxation it is intriguing that the strength and separation from the structural relaxation passes through a maximum for the Br and BF_4 ILs while the strength is diminished for both the smaller Cl and larger PF_6 anions. We also must note that the assumption of time-temperature superposition may not strictly hold for the investigated ILs. For instance, in the dielectric spectra multiple relaxations are observed each with a varying temperature dependence. If such multiple relaxation relaxations with distinct temperature dependence contribute to the mechanical spectra then time-temperature superposition will fail.

Higher temperature flow rheology measurements were also conducted which provide the temperature-dependent zero-shear viscosities. For the non-chloroaluminate ILs, measurements using an Anton-Paar Stabinger viscometer provide additional even higher temperature viscosities. Structural relaxation rates ω_η are
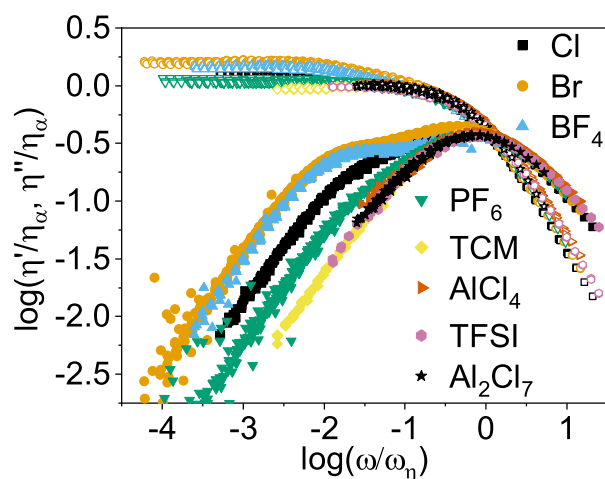
Fig. 9 Real (open symbols) and imaginary parts (closed symbols) of the complex viscosity, $\eta^*(\omega) = \eta'(\omega) + i\eta''(\omega)$.

calculated from the measured viscosities using the Maxwell relation, $\omega_\eta = \frac{G_\infty}{\eta}$, where G_∞ is the high-frequency limiting shear modulus and η is the viscosity. These temperature-dependent rates are presented in Figure 3. The values of G_∞ range from 0.4-0.7 GPa and are provided in the Supplementary Information. The rates thus obtained coincide with the rates measured by oscillatory shear rheology and overlap with the fastest rates obtained from dielectric spectroscopy, $\omega_{M''}$.

4 Conclusions

A thorough investigation of ion dynamics and charge transport in a series of 1-methyl-3-octylimidazolium ionic liquids reveals an anion-structure and temperature dependent separation in localized ion dynamics and the onset of long-range ion diffusion. For the investigated ILs, the separation in rates generally correlates with overall faster ion dynamics, lower calorimetric glass transition temperatures, higher dc ionic conductivities, and lower zero-shear viscosities. These findings indicate an important influence of the local dynamic heterogeneity on charge transport in aprotic ionic liquids. The separation in rate appears to be very sensitive to the organization and specific and non-specific intermolecular interactions within the charge network. In the investigated imidazolium ILs the rates, in general, increasingly separate as the anion becomes larger and more charge diffuse. ILs which are exceptions to this trend may indicate important differences in nearest neighbor packing and interactions. The influence of the cation chemical structure on these factors is evidenced by considering a previously reported series of tributyloctylphosphonium ILs with a comparable series of anions.[37] For these quaternary phosphoniums the separation in rates is almost independent of the identity of the anion. The comparison of imidazolium and phosphoniums, therefore, clearly indicate an important fundamental difference in the ion motions which underlie charge transport of these two IL classes.

Additionally, the strong correlation between the separation in rates and the strengths of the slow sub-α dielectric and slow mechanical relaxations indicate an important influence of local dy-

namic heterogeneity on the dynamics of mesoscale aggregates in aprotic ILs. Increasing separation in rates drives a strong increase in the dielectric strength of the slow, sub-α dielectric relaxation. This result is interpreted in terms of a localized density fluctuation mechanism of the relaxation. The increased mobility of ions within the charge network leads to larger fluctuations in local charge density separated by non-polar domains thus driving an increased polarization across the non-polar domains and thereby increasing the dielectric strength of the sub-α relaxation.

Conflicts of interest

There are no conflicts to declare.

Acknowledgements

Notes and references

1 J. P. Hallett and T. Welton, *Chemical Reviews*, 2011, **111**, 3508–3576.

2 J. G. McDaniel and A. Yethiraj, *Journal of Physical Chemistry B*, 2019, **123**, 3499–3512.

3 R. Hayes, G. G. Warr and R. Atkin, *Chemical Reviews*, 2015, **115**, 6357–6426.

4 T. L. Greaves and C. J. Drummond, *Chemical Society Reviews*, 2013, **42**, 1096–1120.

5 T. Yamaguchi, *Physical Chemistry Chemical Physics*, 2018, **20**, 17809–17817.

6 T. Yamaguchi, *The Journal of Physical Chemistry B*, 2019, **123**, 6260–6265.

7 W. D. Amith, J. C. Araque and C. J. Margulis, *Journal of Physical Chemistry Letters*, 2020, **11**, 2062–2066.

8 F. Philippi, D. Rauber, O. Palumbo, K. Goloviznina, J. McDaniel, D. Pugh, S. Suarez, C. C. Fraenza, A. Padua, C. W. Kay and T. Welton, *Chemical Science*, 2022, **13**, 9176–9190.

9 Y.-L. Wang, B. Li, S. Sarman, F. Mocci, Z.-Y. Lu, J. Yuan, A. Laaksonen and M. D. Fayer, *Chemical Reviews*, 2020, **120**, 5798–5877.

10 J. R. Sangoro and F. Kremer, *Accounts of Chemical Research*, 2012, **45**, 525–532.

11 T. Cosby, Z. Vicars, Y. Wang and J. Sangoro, *The Journal of Physical Chemistry Letters*, 2017, **8**, 3544–3548.

12 A. Shakeel, H. Mahmood, U. Farooq, Z. Ullah, S. Yasin, T. Iqbal, C. Chassagne and M. Moniruzzaman, *ACS Sustainable Chemistry & Engineering*, 2019, **7**, 13586–13626.

13 M. Musiał, S. Cheng, Z. Wojnarowska, B. Yao, K. Jurkiewicz and M. Paluch, *Soft Matter*, 2020, **16**, 9479–9487.

14 J. Gabriel, F. Pabst, A. Helbling, T. Böhmer and T. Blochowicz, *The Scaling of Relaxation Processes*, Springer, Cham, 2018, pp. 203–245.

15 A. E. Khudozhitkov, P. Stange, A. G. Stepanov, D. I. Kolokolov

and R. Ludwig, *Physical Chemistry Chemical Physics*, 2022, **24**, 6064–6071.

16 A. Martinelli, M. Marechal, A. Ostlund and J. Cambedouzou, *Physical Chemistry Chemical Physics*, 2013, **15**, 5510–5517.

17 M. Kofu, M. Nagao, T. Ueki, Y. Kitazawa, Y. Nakamura, S. Sawamura, M. Watanabe and O. Yamamuro, *Journal of Physical Chemistry B*, 2013, **117**, 2773–2781.

18 F. Nemoto, M. Kofu, M. Nagao, K. Ohishi, S. I. Takata, J. I. Suzuki, T. Yamada, K. Shibata, T. Ueki, Y. Kitazawa, M. Watanabe and O. Yamamuro, *Journal of Chemical Physics*, 2018, **149**, 54502.

19 F. Ferdeghini, Q. Berrod, J.-M. Zanotti, P. Judeinstein, V. G. Sakai, O. Czakkel, P. Fouquet and D. Constantin, *Nanoscale*, 2017, **9**, 1901–1908.

20 Q. Berrod, F. Ferdeghini, J.-M. Zanotti, P. Judeinstein, D. Lairez, V. García Sakai, O. Czakkel, P. Fouquet and D. Constantin, *Scientific Reports*, 2017, **7**, 2241.

21 W. D. Amith, J. C. Araque and C. J. Margulis, *Journal of Physical Chemistry Letters*, 2020, **11**, 2062–2066.

22 J. B. Beckmann, D. Rauber, F. Philippi, K. Goloviznina, J. A. Ward-Williams, A. J. Sederman, M. D. Mantle, A. Pádua, C. W. Kay, T. Welton and L. F. Gladden, *Journal of Physical Chemistry B*, 2022.

23 J. Sangoro, T. Cosby and F. Kremer, *Dielectric Properties of Ionic Liquids*, 2016, pp. 29–51.

24 W. D. Amith, J. C. Araque and C. J. Margulis, *Journal of Physical Chemistry B*, 2021, **125**, 6264–6271.

25 R. J. Gale and R. A. Osteryoung, *Molten Salt Techniques*, Plenum Press, New York, 1983, ch. 3, pp. 55–78.

26 J. S. Wilkes, J. A. Levisky, R. A. Wilson and C. L. Hussey, *Inorganic Chemistry*, 1982, **21**, 1263–1264.

27 T. Cosby, M. J. Schnabel, D. P. Durkin, R. A. Mantz and P. C. Trulove, *Journal of The Electrochemical Society*, 2021, **168**, 066515.

28 P. Sippel, S. Krohns, D. Reuter, P. Lunkenheimer and A. Loidl, *Physical Review E*, 2018, **98**, 052605.

29 T. Cosby, A. Holt, P. J. Griffin, Y. Y. Wang and J. Sangoro, *Journal of Physical Chemistry Letters*, 2015, **6**, 3961–3965.

30 T. Cosby, Z. Vicars, M. Heres, K. Tsunashima and J. Sangoro, *The Journal of Chemical Physics*, 2018, **148**, 193815.

31 J. C. Dyre, *Journal Applied Physics*, 1988, **64**, 2456–2468.

32 Yangyang Wang, *Physical Chemistry Chemical Physics*, 2022.

33 J. C. Dyre and T. B. Schrøder, *Reviews of Modern Physics*, 2000, **72**, 873–892.

34 J. R. Sangoro, A. Serghei, S. Naumov, P. Galvosas, J. Karger, C. Wespe, F. Bordusa and F. Kremer, *Physical Review E*, 2008, **77**, 51202.

35 M. Heres, T. Cosby, E. U. Mapesa and J. Sangoro, *ACS Macro Letters*, 2016, **5**, 1065–1069.

36 C. Gainaru, E. W. Stacy, V. Bocharova, M. Gobet, A. P. Holt, T. Saito, S. Greenbaum and A. P. Sokolov, *The Journal of Physical Chemistry B*, 2016, **120**, 11074–11083.

37 T. Cosby, Z. Vicars, E. U. Mapesa, K. Tsunashima and J. Sangoro, *The Journal of Chemical Physics*, 2017, **147**, 234504.

38 P. Pal and A. Ghosh, *Physical Review E*, 2015, **92**, 062603.

39 J. H. Ambrus, C. T. Moynihan and P. B. Macedo, *Journal of Physical Chemistry*, 1972, **76**, 3287–3295.

40 K. Pathmanathan and G. P. Johari, *Journal of Chemical Physics*, 1991, **95**, 5990–5998.

41 P. J. Griffin, A. P. Holt, K. Tsunashima, J. R. Sangoro, F. Kremer and A. P. Sokolov, *Journal of Chemical Physics*, 2015, **142**, 84501.

42 W. Xu, E. I. Cooper and C. A. Angell, *Journal of Physical Chemistry B*, 2003, **107**, 6170–6178.

43 F. Kremer and A. Schönhals, *Broadband Dielectric Spectroscopy*, Springer, Berlin, 2003, p. 729.

44 E. I. Izgorodina, M. Forsyth and D. R. MacFarlane, *Physical Chemistry Chemical Physics*, 2009, **11**, 2452–2458.

45 T. Cosby, U. Kapoor, J. K. Shah and J. Sangoro, *The Journal of Physical Chemistry Letters*, 2019, **10**, 6274–6280.

46 A. Triolo, O. Russina, H. J. Bleif and E. Di Cola, *Journal of Physical Chemistry B*, 2007, **111**, 4641–4644.

47 C. Hardacre, J. D. Holbrey, C. L. Mullan, T. G. A. Youngs and D. T. Bowron, *Journal of Chemical Physics*, 2010, **133**, 74510.

48 O. Russina, A. Triolo, L. Gontrani, R. Caminiti, D. Xiao, L. G. Hines, R. A. Bartsch, E. L. Quitevis, N. Plechkova and K. R. Seddon, *Journal of Physics: Condensed Matter*, 2009, **21**, 424121.

49 T. Pal and M. Vogel, *ChemPhysChem*, 2017, **18**, 2233–2242.

50 R. Richert, *Journal of Physics: Condensed Matter*, 2002, **14**, R703.